Is there a robust effect of anthropogenic aerosols on the Southern Annular Mode?

Article

Published Version

AGU PUBLICATIONS

JGR

Journal of Geophysical Research: Atmospheres

RESEARCH ARTICLE
10.1002/2015JD024218

Is there a robust effect of anthropogenic aerosols on the Southern Annular Mode?

H. Steptoe[1,2], L. J. Wilcox[1,3], and E. J. Highwood[1]

[1]Department of Meteorology, University of Reading, Reading, UK, [2]Met Office, Exeter, UK, [3]National Centre for Atmospheric Science (Climate), Reading, UK

Key Points:
- The SAM response to anthropogenic aerosols is not robust
- A significant negative SAM response to anthropogenic aerosols is seen in some realizations
- Assuming that responses to forcing are linearly additive may overstate the role of aerosol

Supporting Information:
- Supporting Information S1
- Figures S1

Correspondence to:
H. Steptoe,
hamish.steptoe@metoffice.gov.uk

Citation:
Steptoe, H., L. J. Wilcox, and E. J. Highwood (2016), Is there a robust effect of anthropogenic aerosols on the Southern Annular Mode?, *J. Geophys. Res. Atmos.*, *121*, 10,029–10,042, doi:10.1002/2015JD024218.

Received 11 SEP 2015
Accepted 18 JUL 2016
Accepted article online 22 JUL 2016
Published online 13 SEP 2016

Abstract Historical anthropogenic aerosol (AA) changes are found to have caused a statistically significant negative Southern Annular Mode (SAM) trend (associated with an equatorward jet shift) in 14 out of 35 individual ensemble members from the fifth Coupled Model Intercomparison Project (CMIP5) since 1860. However, this response is not robust. The significance of the SAM response to aerosol is model dependent and not simply related to aerosol forcing. Multiple sources of uncertainty result in a nonrobust response that means that the model mechanism connecting remote Northern Hemisphere AA forcing remains unclear. Analysis of single forcing experiments suggests that assuming the climate response to individual model forcings to be linearly additive cannot be made without proper assessment. Our results suggest that AAs may have had a historical influence on the SAM, but its influence may be overstated by assuming linearity.

1. Introduction

In recent decades, significant changes to Southern Hemisphere (SH) atmospheric circulation have been observed, particularly in the Austral summer (December–February, DJF) [*Thompson et al.*, 2011]. These circulation changes include a poleward shift of the jets [e.g., *Ceppi and Hartmann*, 2013; *Solman and Orlanski*, 2014], a positive SAM index trend [e.g., *Marshall*, 2003], and a poleward expansion of the Hadley cell [*Choi et al.*, 2014; *Quan et al.*, 2014] and subtropical dry zones [*Cai et al.*, 2012].

The SAM, after *Limpasuvan and Hartmann* [1999], describes the dominant mode of atmospheric variability in the SH. It represents the poleward-equatorward shift of momentum and mass across the SH midlatitudes, at high- and low-frequency time scales, in a near-zonally symmetric pattern. The observed positive trend in the SAM index and the poleward trend in the position of the jet stream have been linked to increases in the upper troposphere-lower stratosphere meridional temperature gradient [*Chiang and Friedman*, 2012; *Wilcox et al.*, 2012; *Gerber and Son*, 2014]. Such increases have been driven by increases in greenhouse gases (GHGs), which act to cool the polar lower stratosphere and warm the tropical upper troposphere, and by decreases in stratospheric ozone (sO_3), which act to cool the polar lower stratosphere. In DJF, when the influence of sO_3 depletion on the troposphere is greatest [*Thompson and Solomon*, 2002], sO_3 depletion has a dominant influence on austral jet trends [e.g., *Gerber and Son*, 2014; *Polvani et al.*, 2011a; *Lee and Feldstein*, 2013].

The influence of sO_3 on SAM trends is time dependent. The sO_3 depletion since the mid-twentieth century has reinforced circulation changes associated with increasing GHGs [*Shindell and Schmidt*, 2004], and a particularly rapid depletion in recent decades has caused the sO_3 influence to dominate [*Gerber and Son*, 2014]. In contrast, the anticipated 21st century recovery of sO_3 will act to oppose the effects of increasing GHGs [*Polvani et al.*, 2011b]: warming the polar lower stratosphere, reducing the meridional temperature gradient, and pushing the SAM toward its negative phase. Estimates of ozone recovery suggest a turnaround in total column ozone occurred circa 2005, with a relatively constant rate of recovery expected to return ozone concentrations to 1980 levels between 2030 and 2040 [*Pawson et al.*, 2014]. Previous studies [e.g., *Polvani et al.*, 2011b; *Wang et al.*, 2014] project that there will be a cancelation between these opposing influences on SH circulation, resulting in small trends, in the coming decades.

With the anticipated compensation between the effects of increasing GHGs and sO_3 on the SAM, it is possible that other forcings may play a more prominent role in decadal-scale SAM variability in the near term. In order to understand whether AA is likely to have a marked effect on near-term SAM trends, it is important to understand whether the large historical changes in AA had an influence on the SAM and, if so, the mechanisms

by which this influence arose. In this paper we focus on determining whether the effects of AAs on the SAM were significant and robust in the historical period. SH circulation changes previously attributed to AA forcing include a decrease in sea level pressure at high latitudes [*Gillett et al.*, 2013], a decrease in surface air temperature in the South Pacific [*Xie et al.*, 2013], and a decrease in the midtropospheric temperature gradient which contributes to a weakening of the SH subtropical jet [*Rotstayn et al.*, 2013]. *Rotstayn* [2013] demonstrated that AAs induced a slight negative SAM trend in the past (1950 to 2005) in CSIRO-Mk3.6.0. We will examine whether such a response is robust across a selection of the models in CMIP5.

AAs can affect the climate directly through their interaction with radiation or indirectly via their effects on clouds. The effects of aerosols on clouds include an increase in droplet number and albedo in response to increasing aerosol concentrations (the first aerosol indirect effect [*Twomey*, 1977]) and an increase in cloud lifetime as a result of the reduced precipitation efficiency of smaller cloud droplets (the second indirect effect [*Albrecht*, 1989]). These effects primarily act to reduce the amount of shortwave radiation reaching the Earth's surface. Hence, model simulations suggest that the known increase in atmospheric aerosols over the industrial era has caused a negative radiative forcing and a decrease in global-mean near-surface temperature (Figure 1a) [*Boucher et al.*, 2013]. However, there is considerable uncertainty over the magnitude of aerosol radiative forcing, particularly that caused by aerosol-cloud interactions, due to uncertainties in preindustrial aerosol concentrations and model representations of aerosol processes [*Carslaw et al.*, 2013; *Wilcox et al.*, 2015].

Global aerosol loads (including sulphate, nitrates, and black carbon) have increased through most of the industrial era, with particularly rapid increases in the mid-twentieth century (Figure 1b). Global aerosol loading is now beginning to decrease [*Mao et al.*, 2014] as a result of air quality concerns. Aerosol is projected to continue to decrease in future, although the rate and magnitude of this decrease varies greatly across different scenarios [*van Vuuren et al.*, 2011; *Kloster et al.*, 2008].

AA forcing is predominantly confined to the NH, where most emissions occur [e.g., *Zelinka et al.*, 2014]. The mechanisms by which this may induce a circulation change in the SH are currently uncertain. *Rotstayn* [2013] and *Ceppi et al.* [2013] suggest interhemispheric coupling occurs via the Hadley circulation, as they find maximal AA forcing collocates with the descending branch of the Hadley Cell, but *Cai et al.* [2006] suggest that ocean-atmosphere interactions redistribute AA forcing-induced temperature changes via cross-equatorial oceanic heat transport in the Atlantic and Pacific. Some studies have found that despite the different patterns in radiative forcing in response to AA and GHG increases, spatial patterns of the sea surface temperature and precipitation [*Xie et al.*, 2013] and temperature and wind [*Rotstayn et al.*, 2013] responses are similar. However, these conclusions still remain model and variable dependent, with *Gillett et al.* [2013] finding distinct patterns in the observed sea level pressure response to AA and GHG changes (consistent with positive and negative SAM responses, respectively).

In this paper, we investigate the significance of AA forcing on historical SAM variability using the CMIP5 multimodel data set. Individual model trends will be discussed in the context of the diverse representation of aerosol processes in climate models. We then discuss the implications of assuming a linear paradigm for combined forcings.

2. Data

This study uses data from a subset of 19 models, as available at the time of writing, from CMIP5, described in Table 1. Fourteen models include representations of both aerosol radiation interactions (ERFari) and aerosol-cloud interactions (ERFaci, either the first or the second effects). All models use the same aerosol emissions [*Lamarque et al.*, 2010]. However, differences in transport and aerosol removal processes across the models mean that the aerosol quantity and distributions in the models are very diverse [*Wilcox et al.*, 2015]. These differences, in addition to variability in the representation of aerosol-cloud interactions, and in the model cloud fields themselves [*Zelinka et al.*, 2014; *Wilcox et al.*, 2015], contribute to further diversity in the radiative forcing due to AAs across the models.

Data for the historical experiments (1850 to 2005), referred to as the all-forcing ensemble (AF) throughout, is used from 19 models (Table 1). Seventeen of these also provide a GHG-only forcing experiment (historicalGHG, the greenhouse gas ensemble, and GHG), and we include 10 model simulations forced only by time-varying

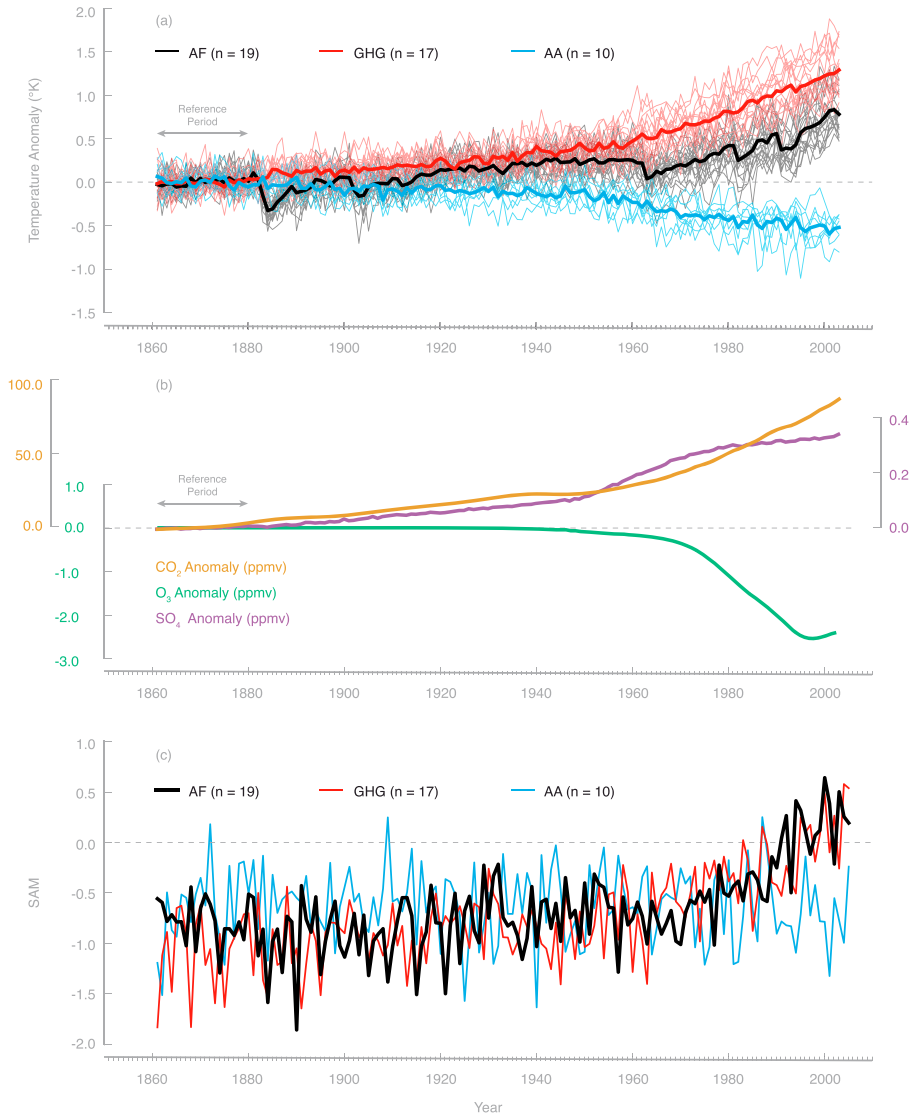

Figure 1. (a) Change in global-mean DJF-mean surface temperature for each forcing experiment relative to 1861–1881 mean, (b) changes in CO_2 [*Meinshausen et al.*, 2011], Antarctic O_3 at 50 hPa [*Cionni et al.*, 2011] and SO_4 relative to their 1860–1880 means value, and (c) multimodel mean DJF-mean SAM index for each of the first ensemble members for each forcing experiment. For Figure 1b, we use vertically integrated sulphate load to relate changes in aerosols to forcing, as sulphate accounts for most of the mass of aerosol, and is a good predictor of the indirect effect [*Wilcox et al.*, 2015]. Note that the spread in sulphate concentration between models is significant [see, for example, *Wilcox et al.*, 2015]. Also note that for Figure 1a the means each have a different number of members, indicated in brackets. Lines in Figures 1b and 1c represent multimodel means.

AA (the anthropogenic aerosol ensemble, AA, referred to by CMIP5 as historicMisc experiments and identified by the physics *p* suffix). At the time of analysis, ozone-only simulations were unfortunately unavailable for any of these subsets of models. Where multiple ensemble members are available, we use the *r* suffix of the CMIP naming convention [*Taylor et al.*, 2012] to refer to individual ensemble members.

Different numbers of ensemble members are typically available for each simulation (Table 1). We include only the first member from each model in multimodel means to avoid giving extra weight to any single model. When analyzing the temporal characteristics of a given time series, we treat each ensemble member individually; taking model ensemble means would enhance the signal-to-noise ratio, making models with large ensembles more likely to return significant results in intermodel comparisons.

Table 1. CMIP5 Models Used in This Study[a]

			Model Experiments			Indirect Effects	
Institute	Model	Reference	AF	GHG	AA	First	Second
BCC	BCC-CSM1.1 [b]	*Wu et al.* [2010]	3	1			
BCC	BCC-CSM1.1(M) [b]	*Wu et al.* [2010]	3				
GCESS	BNU-ESM [b]	*Ji et al.* [2014]	1	1			
CCCMA	CanESM2	*Chylek et al.* [2011]	5	5	5 (−0.87 Wm^{-2})	[c]	
NCAR	CCSM4 [b]	*Gent et al.* [2011]	6	3	3		
NSF-DOE-NCAR	CESM1-CAM5	*Hurrell et al.* [2013]	3	1	3	[c]	[c]
CNRM-CERFACS	CNRM-CM5	*Voldoire et al.* [2012]	10	2		[c]	
CSIRO-QCCCE	CSIRO-Mk3.6.0	*Rotstayn et al.* [2012]	10	10	10 (−1.40 Wm^{-2})	[c]	[c]
NOAA GFDL	GFDL-CM3	*Donner et al.* [2011]	5	5	3 (−1.60 Wm^{-2})	[c]	[c]
NOAA GFDL	GFDL-ESM2M [b]	*Dunne et al.* [2012]	1	1	1		
NASA GISS	GISS-E2-R	*Schmidt et al.* [2014]	6	5	5	[c]	[c]
MOHC	HadGEM2-ES	*Jones et al.* [2011]	4	4	3 (−1.24 Wm^{-2})	[c]	[c]
IPSL	IPSL-CM5A-LR	*Dufresne et al.* [2013]	5	3	1 (−0.72 Wm^{-2})	[c]	
IPSL	IPSL-CM5A-MR	*Dufresne et al.* [2013]	3	3		[c]	
MIROC	MIROC5	*Watanabe et al.* [2010]	5			[c]	[c]
MIROC	MIROC-ESM	*Watanabe et al.* [2011]	3	3		[c]	[c]
MIROC	MIROC-ESM-CHEM	*Watanabe et al.* [2011]	1	1		[c]	[c]
MRI	MRI-CGCM3	*Yukimoto et al.* [2012]	5	1		[c]	
NCC	NorESM1-M	*Iversen et al.* [2013]	3	1	1 (−0.99 Wm^{-2})	[c]	[c]
		TOTAL	82	50	35		

[a]Numbers indicate the number of members used from each model ensemble, but note that the number of members used is not necessarily the total number of members available. Where model data are available for sstClim and sstClimAerosol experiments, we show the global AA effective radiative forcing in brackets.
[b]Models that only include ERFari effects.
[c]Models that include ERFaci effects.

3. Data Analysis

The data analysis methodology comprises the following: (1) calculation of the SAM index, (2) a method to decompose this time series into trends on different timescales, and (3) an analysis of the significance of these trends. All analysis will focus on DJF, as this is the season with the largest tropospheric response to sO_3 depletion and therefore the only season where a cancelation between the effects of increasing GHG and decreasing sO_3 can be expected. As such, this is the only season where a response to AAs may play a role in determining the sign of the SAM trend in the near future. No clear seasonality was seen in the response to AAs themselves (not shown).

3.1. SAM Index

The SAM index is calculated using the method of *Gong and Wang* [1999], who define the SAM as the difference between the normalized zonal mean pressure at 40°S and 65°S, such that

$$\mathrm{SAM} = P^*_{40°S} - P^*_{65°S} \tag{1}$$

where P^* represents the normalized monthly zonal mean sea level pressure:

$$P^* = \frac{P - \bar{P}}{S_n(P)} \tag{2}$$

where P is zonal mean pressure, $\bar{P}$ is the time mean, and $S_n(P)$ is the uncorrected sample standard deviation for the number of years (n). *Ho et al.* [2012] show that an index based on the *Gong and Wang* [1999] method and an EOF-based method are very strongly correlated. In light of this strong relationship, we anticipate intermodel differences in the SAM response to much greater than any differences related to the choice of definition and so only present results from the *Gong and Wang* [1999] definition.

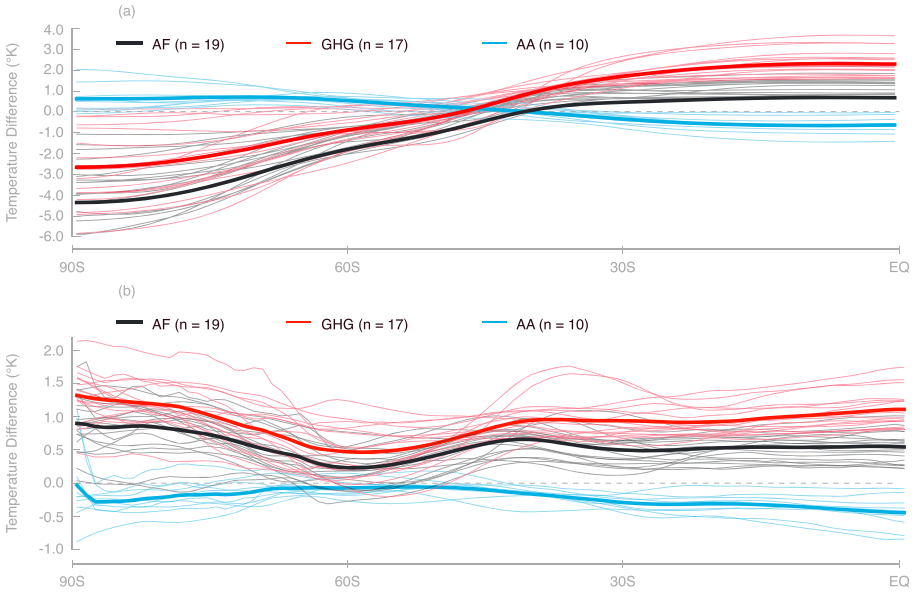

Figure 2. Zonal-mean DJF-mean temperature anomalies between the present day (1983–2003) and preindustrial (1861–1881) periods at (a) 200 hPa and (b) near the surface. Bold lines represent the multimodel mean.

3.2. Ensemble Empirical Mode Decomposition

Ensemble empirical mode decomposition (EEMD) is an empirical frequency decomposition technique proposed by *Wu and Huang* [2004, 2009]. Its key advantage is that it is capable of extracting the frequency components from a nonlinear nonstationary process [e.g., *Wu et al.*, 2007]. The technique decomposes a time series into a set of intrinsic mode functions (IMFs), each describing a given frequency mode of the data, and a residual. Once all frequency modes are separated out of the data, the residual from the EEMD process represents the long-term trend. As the process retains the time-varying nature of the signal frequency, signal peaks, and troughs can be interpreted in the context of physical climate drivers. EEMD is adaptive to a variety of climate data [e.g., *Franzke*, 2013; *Wilcox et al.*, 2013; *Franzke et al.*, 2012; *Franzke*, 2012; *Chang et al.*, 2011] and has successfully been applied for the purpose of SAM trend analysis in previous studies [e.g., *Franzke*, 2009; *Pohl et al.*, 2010].

The use of EEMD for our trend analysis allows us to avoid the use of linear trends for either the whole time series or the components of it where a certain forcing is expected to drive a change. We expect the largest historical influence of AA on the SAM to occur in the mid-twentieth century, when its impact on global climate was greatest [*Wilcox et al.*, 2013]. However, the representation of aerosol processes, and the climate responses to them, is diverse. We therefore avoid the use of linear trends with arbitrary endpoints as the most suitable endpoints are likely to differ between models. EEMD allows for significance testing of nonlinear trends without a need for subjective thresholds, as described in the supporting information.

4. Results

The time evolution of GHG, sO_3, and AA are different. GHG concentrations (based on CO_2 model diagnostic) increase monotonically during the historical period. the sO_3 decreases during the latter half of the twentieth century, with a more rapid rate of depletion in recent decades. Global mean AA concentrations (based on SO_4 model diagnostic) increased rapidly in the mid-twentieth century, with a smaller steady rise from 1970 onward (Figure 1b). As such, they are expected to imprint different temporal signatures on the SAM (Figure 1c). Different temperature responses to GHG and AA can clearly be seen in Figure 2, which shows temperature anomalies between the present day and preindustrial periods near the surface and at 200hPa. GHGs induce a warming in the tropics at 200hPa, and a cooling at high latitudes, which acts to increase the meridional temperature gradient. This pattern is largely reflected in the all forced response, while AAs induce the opposite response but smaller in magnitude. Near the surface, AAs cause cooling at most latitudes while GHGs cause warming. In both cases, the temperature changes are smaller near 60°S.

Long-term trends should be well captured by the residual from EEMD. The influence of AAs and sO_3 may have a multidecadal signature more likely to be seen in the last IMF. However, we find the last IMF of the SAM to be poorly resolved by EEMD and do not consider it further. We treat the residual as a good representation of the forced change in the SAM when it is found to be significantly different to a residual that might be expected from an equivalent noise time series (following the methodology described in the Supporting Information).

4.1. Long-Term Trends

The residuals from EEMD, representative of the long-term trend in the SAM, are shown in Figure 3 for each model and experiment. Residual all-forcing (AF) trends predominantly show the SAM index becoming increasingly positive over the historical period. BNU-ESM and HadGEM2-ES show the smallest change in SAM index over this period. In HadGEM2-ES, for which single forcing experiments are available, this appears to be due, at least in part, to cancelation between the response to GHG and to AA. For all models, GHG trends move toward an increasingly positive SAM phase throughout the historical period, similar to AF trends. AA trends show a decrease in the latter half of the historical period for at least one ensemble member in all models except CCSM4, GFDL-ESM2M and NorESM1-M, which show no trend, or even a small positive trend.

The response of the SAM to AA can be seen to mirror the response to GHG in the multimodel mean, although the amplitude of the response is smaller in the AA case, about one third the magnitude of that to GHG (Figure 3). The historical AF trend simulated by models that only include ERFari effects is slightly larger than that from models that include both ERFari and ERFaci. This difference is small, but consistent, with the differences in global temperature trends from the two groups of models (models with a representation of the direct effect only show greater warming than those without) and may be indicative of a greater reduction in the AF trend from AA in models with a representation of ERFaci [*Wilcox et al.*, 2013], although we are only able include two ERFari models here (CCSM4 and GFDL-ESM2M).

The r1 ensemble member for each model, which we use to calculate the CMIP5 mean, is highlighted in Figure 3. For models where more than one ensemble member is available, it can be seen that r1 is not always the member most representative of a given model's response to forcing. In CanESM2 and CSIRO-Mk3.6.0 in particular, the first ensemble member shows the smallest response to AA forcing.

The multimodel mean trends, and those from several individual models, suggest that the change in SAM due to GHG is not dissimilar to that due to AF. The sO_3 has been shown to have a dominant influence on jet position compared to GHG in a comparable set of models [*Polvani et al.*, 2011b, 2011a]. It is therefore not unreasonable to expect the AF trend to be greater than that due to GHGs alone. The similarity of the two responses, which is seen in both the raw (Figure 1c) and the filtered data (Figure 3), suggests that either the SAM is not as strongly influenced by sO_3 changes as the jet, the SAM response to a combination of forcings may not be well represented by the linear sum of the response to these forcings individually, or that there is too much sampling variability. The potential nonlinearity in the SAM response to forcing will be investigated further in section 4.3.

4.2. Significance Testing

In order to determine whether the trends shown in Figure 3 represent a forced response, they must be considered alongside a significance test. Figure 4 summarizes the significance of the residual EEMD trend for each model ensemble member, determined using the methodology described in detail in the supporting information. The residual is significant at the 5% level for most models for both the AF and GHG experiments. The response to GHG is typically more strongly significant than the response to AF. Note that none, bar one, of the r1 ensemble members produce a significant ($\geq$10%) residual in response to AA forcing. Only considering the first ensemble member would underestimate of the magnitude of the response to AA forcing.

Examination of the all-forcing simulations shows that 17 of 19 models have at least one ensemble member with a significant ($\geq$10%) positive trend in the SAM index. This is consistent with previous observational studies [e.g., *Visbeck*, 2009; *Marshall*, 2003] and investigations using CMIP3 models [e.g., *Fogt et al.*, 2009; *Cai and Cowan*, 2007].

Almost all individual ensemble members have significant trends in response to GHG forcing. In all models, the majority of members are significant, demonstrating a robust response of the SAM to GHG forcing. The majority of members also produce significant residual trends in the AF experiment, at both the 10% and 5% levels. This is true for the CMIP ensemble as a whole, and for individual models, except for HadGEM2-ES and

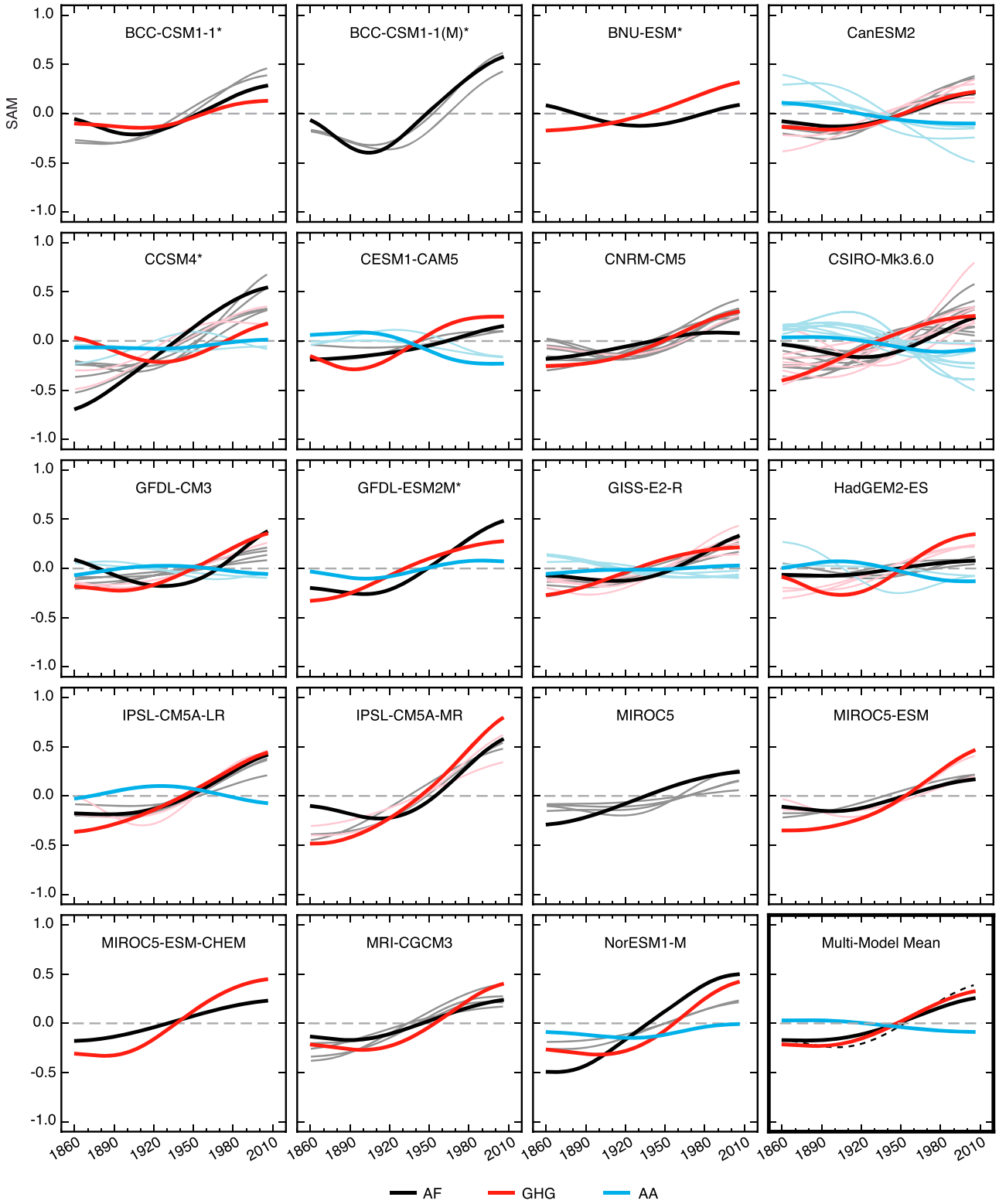

Figure 3. DJF-mean residual EEMD trends for each model ensemble for all-forcing (AF, black), GHG (red), and AA (blue) model experiments. Darker, thicker lines show the *r1* ensemble member, and lighter lines show the other ensemble members. Models that only include ERFari effects are marked with asterisks and are included separately in the multimodel mean (black dashed line). Note that the multimodel mean is derived from all ensemble members.

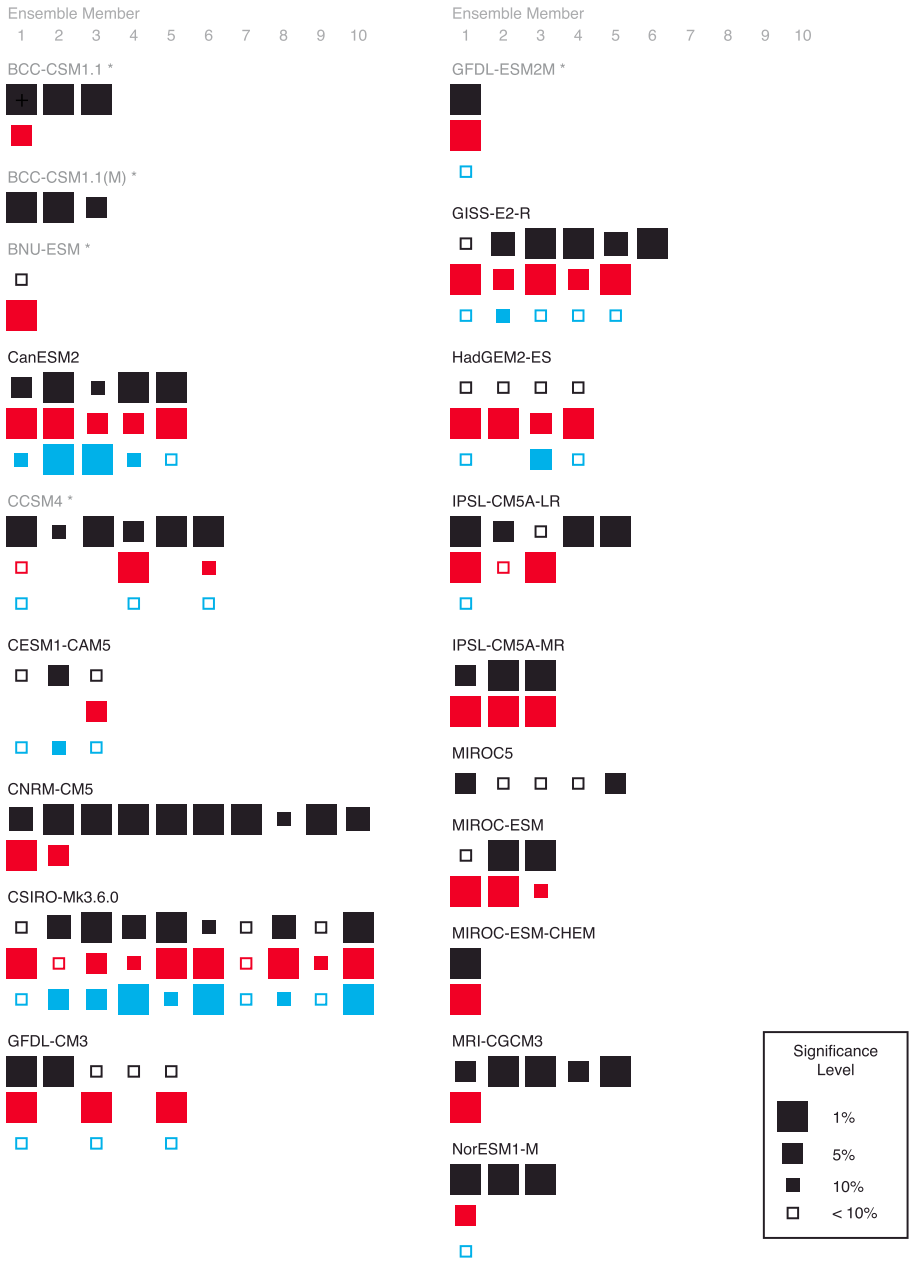

Figure 4. Significance of all model ensemble members for all-forcing experiments (black), GHG experiments (red), and AA experiments (blue) residual EEMD trends, for the period 1860–2005. The size of the square represents the significance level: large 1%, medium 5%, and small 10%. Open squares represent a significance level <10 %. Models that only include ERFari effects are marked with asterisks. For significant model members, AF and GHG trends are always positive and AA trends are always negative.

BNU-ESM where no AF members have a significant trend in the residual. In CESM1-CAM5, GFDL-CM3, and MIROC5, only a minority of members have significant AF trends.

It can be seen in Figures 3 and 4 that the magnitude and significance of the response to AA can vary considerably across members of the same model, indicating uncertainty in the response. However, both CanESM2 and CSIRO-Mk3.6.0 simulate a long-term trend in response to AA forcing that is significant at the 10% level or greater in 4 out of 5 and 7 out of 10 of their available ensemble members, respectively (Figure 3). Additionally, both models include members that simulate a response that is significant at the 1% level. We suggest this indicates that there is a robust and significant SAM response to AA forcing in these models. This is consistent

with the results of *Rotstayn* [2013] who suggested that AA are likely to influence the sign of future SAM trends in CSIRO-Mk3.6.0.

HadGEM2-ES also has a strong response in one of its AA ensemble members (5% level). The other seven models for which AA simulations have been analyzed (CCSM4, CESM1-CAM5, GFDL-CM3, GFDL-ESM2M, GISS-E2-R, IPSL-CM5A-LR, NorESM1-M) do not show robust responses.

It is possible that the diverse SAM response to AA forcing is related to the large range of aerosol radiative forcing simulated in the models. Such a diverse response arises because specifying emissions results in diverse aerosol concentrations and distributions in the models, which is then amplified by the use of different parameterizations of aerosol-cloud interactions and diverse cloud fields [*Wilcox et al.*, 2015]. For the six models where data is available for sstClim (a control run with climatological sea surface temperatures and sea ice imposed) and sstClimAerosol (the same, but with year 2000 aerosol) experiments, we calculate the global AA effective radiative forcing (ERF, shown in Table 1) between 1850 and 2000. Applying the assumption that each ensemble member from a given model has the same radiative forcing to allow us to use trends from all available ensemble members, we calculate the Pearson correlation between effective radiative forcing (ERF) and the 1950–2000 SAM trend. We find that the strength and significance of SAM trends in response to AA forcing cannot be predicted based on the magnitude of AA ERF ($r = -0.19$).

Previous studies have shown a relationship between trends in the SAM index and trends in meridional temperature gradient [e.g., *Thompson and Solomon*, 2002] and jet position [e.g., *Ceppi and Hartmann*, 2013]. Following *Wilcox et al.* [2012], we define the meridional temperature gradient as the difference between polar average lower stratospheric temperature (150 hPa, 75–90°S) and tropical upper tropospheric temperature (250 hPa, 0–25°S). Using all available members, we find that the relationship between the trends in the meridional temperature gradient and in the SAM is strong in the historical AA experiments for the six models where we are able to calculate ERF ($r = 0.93$). However, the relationship between ERF and the meridional temperature gradient is weak ($r = -0.15$), further suggesting that the magnitude of the SH circulation response to AA does not have a simple relationship to global ERF. In part, this relationship may be being obscured by the influence of internal variability on the SAM trends. *Ceppi et al.* [2014] show that differences in the meridional gradient of absorbed shortwave radiation are likely to be the cause, not the result, of differences in jet response between models. This may further explain why ERF alone cannot explain intermodel differences in SAM response.

Kidston and Gerber [2010] identified a relationship between the magnitude of the shift in the SH jet and the initial position of the jet in CMIP3 models, which is also present in CMIP5 models [*Wilcox et al.*, 2012]. While there was no relationship between 1860–1900 mean SAM and the 1950–2000 SAM trend in the models we consider here, there was a strong relationship between 1860–1900 meridional temperature gradient and the meridional temperature gradient trend ($r = 0.80$). This suggests that model climatology may also play a role in the circulation response to AA, which may contribute to the lack of a linear relationship between ERF and the SAM response to AA changes.

In addition to potentially being obscured by the influence of model biases, the SAM response to AA is also likely to be influenced by ocean transport, which is one mechanism by which NH AA forcing may be felt in the SH. *Frölicher et al.* [2015] show that there is substantial variation in both ocean heat uptake and northward excess heat transport among CMIP5 models, particularly around 40°S. This suggests a lack of model consensus on the mechanism and driving changes that alter the surface energy budget since preindustrial times, which makes it difficult to disentangle a weak aerosol signal.

We find a strong relationship between SAM and meridional temperature gradient trends in historical AA. However, we are unable to identify a relationship between ERF for AA and either changes in meridional temperature gradient or changes in SAM. This is consistent with finding the most robust responses to AA in CanESM2 and CSIRO-Mk3.6. CanESM2 has relatively small ERF for our sample, while CSIRO has quite a large ERF. Lack of a simple relationship between forcing and response suggests that the mechanism by which NH aerosol affects SH is important for determining the magnitude of the model response. For example, if ocean transport is the main driver in models, then biases in this process are likely linked to the magnitude of SAM response. Additionally, the SAM has a large amount of internal variability, and we are looking for a signal that is small in comparison. We cannot rule out the possibility that a larger ensemble would show a stronger relationship between ERF and SAM.

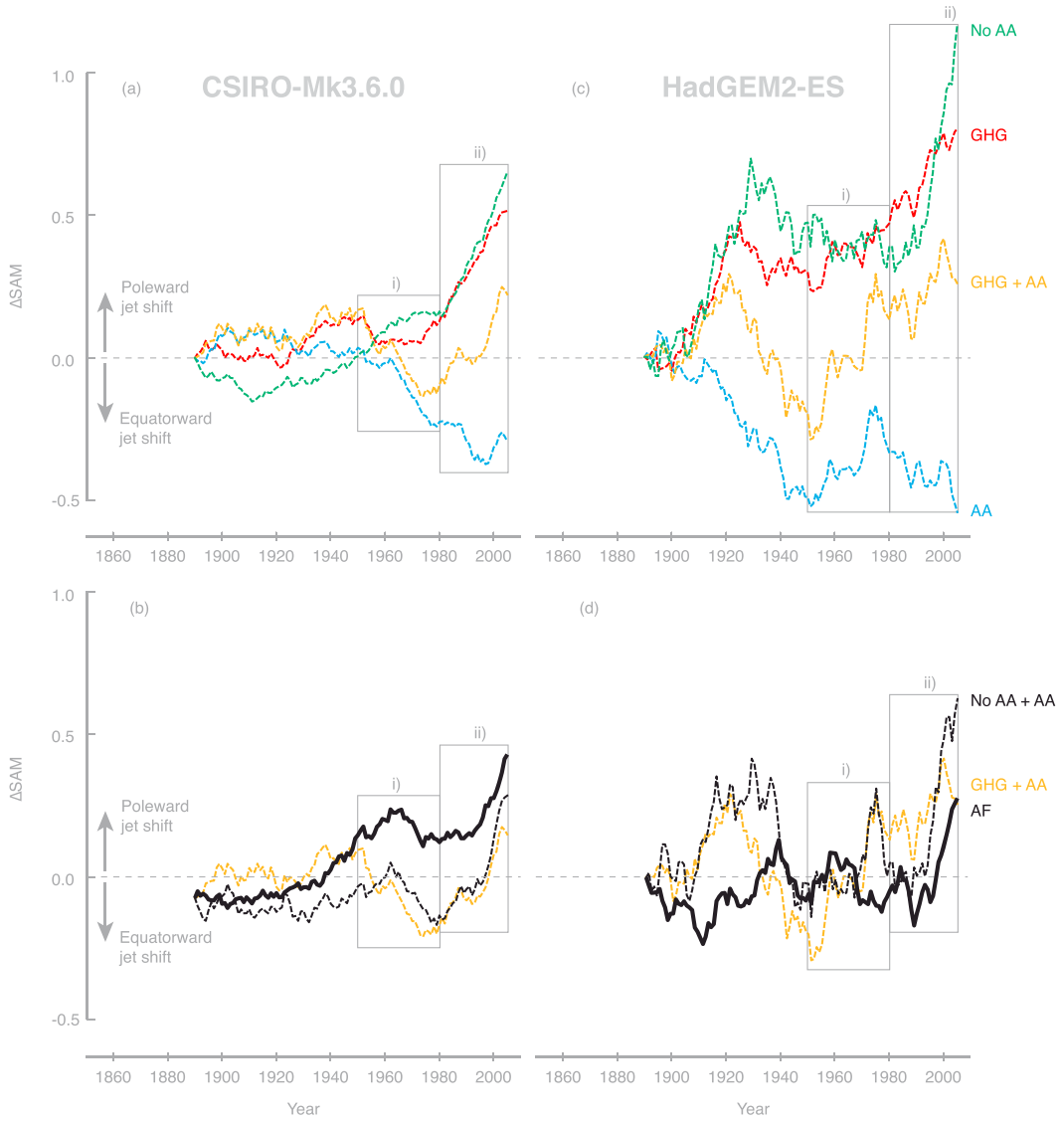

Figure 5. Comparison of *CSIRO-Mk3.6.0* and *HadGEM2-ES* single and combined forcing trends. (a, c) Comparison of the sum of the responses to GHG and AA (GHG+AA, yellow line), the GHG experiment (red line), the AA experiment (blue line), and the NoAA experiment (green line). (b, d) Comparison of the historical AF experiment (black solid line) with NoAA + AA (black dashed line), and GHG+AA. Each time series is the 30 year running mean of a 10-member (CSIRO-Mk3.6.0) or 3-member (HadGEM2-ES) ensemble mean for DJF only, from 1860 to 2005. Note that the time-varying trends represent the change in SAM from the 1890 reference and are not observed SAM values. Boxes (i) and (ii) are periods over which linear regression is performed, summarized in Tables S1 and S2 in the supporting information.

4.3. Comparison of Single Forcings

Investigating the CSIRO-Mk3.6.0 and HadGEM2-ES models, we attempt to quantify the relative importance of AA and GHGs to trends in the SAM. In addition to the AF, AA, and GHG experiments, we use an additional forcing experiment: NoAA, equivalent to AF forcing scenario but with AA fixed at 1860 levels. All other forcings are time varying.

We also use two combinations of results from experiments: (1) GHG+AA, a linear sum of GHG and AA, and (2) AA+NoAA, a linear sum of AA and NoAA experiments.

If the response to the single forcings combine linearly, AA+NoAA should produce a SAM index evolution similar to the AF experiment. If the response is found to be linear, a quantitative estimate of the relative contribution of AA and GHG to the AF run can be formulated.

Figures 5a and 5c show the 30 year running mean of the ensemble mean GHG, AA, and NoAA experiments, and GHG+AA combination for CSIRO-Mk3.6.0 and HadGEM2-ES. Figures 5b and 5d focus on the AF experiment and NoAA+AA and GHG+AA combinations for the same period. Trend analysis has been performed on these time series for two periods: 1950–1980 and 1980–2005. We expect to see the largest influence of AA in 1950–1980, related to the rapid increase in global aerosol concentrations in this period, and trends driven primarily by GHG and sO_3 changes in 1980–2005.

In CSIRO-Mk3.6.0, AA drives a decrease in the SAM index from 1950 (Figure 5a). This is particularly large between 1950 and 1980. In this period there is no trend in the SAM due to GHGs and a small positive trend in the NoAA experiment, suggesting that AAs are likely to be the main driver of the trend in this period in CSIRO-Mk3.6.0. From 1980, the rate of change in the SAM due to AA is smaller, around a quarter of the magnitude of the GHG trend (Tables S1 and S2 in the supporting information). Interestingly, there is almost no difference between the NoAA and GHG series in this period, when sO_3 might be expected to be the main driver of the trend. This indicates that either the response to sO_3 depletion in this model is small or the response is not linearly additive.

Assessing the significance of differences between forcing trends (Tables S3 and S4 in the supporting information) using a parametric bootstrapping approach [*Davison and Hinkley*, 1997], we find that the NoAA+AA and AF experiments have significantly different trends in both periods (Figure 5b), demonstrating that the linear combination of the response to single forcings is not a good assumption in this case. This is contrary to the findings of *Rotstayn* [2013] who did find linearity to be a good assumption for CSIRO-Mk3.6.0. However, there are differences in the methodology used, e.g., in the SAM metric and time period, so it is possible that the extent of nonlinearity is also dependent on methodology.

Time series of the SAM anomaly from HadGEM2-ES experiments are shown in Figures 5c and 5d. Fewer ensemble members were available for this model (3 members compared to 10 for CSIRO). Consequently, a greater amount of variability is seen on short timescales in addition to the forced response. In addition to this variability, there also appears to be internally driven multidecadal-scale variability in the 30 year running means. There is a large positive trend in the SAM index, followed by a decrease, in response to GHG early in the historical period, which, as it bears no resemblance to the temporal evolution of GHG concentrations in that period (Figure 1b), is unlikely to be a forced response. The multidecadal variability in the AA experiment appears to be similarly influenced by internal variability.

The apparent influence of internal variability in the HadGEM2-ES running means make it difficult to assess the contributions of each forcing component to the total response. Furthermore, it is difficult to make a statement about the validity of the assumption that the AF response is well represented by the linear sum of the responses to single forcings. The AF and NoAA+AA trends were found to be significantly different in both time periods (Table S4 in the supporting information), but any linearity in the true forced response will be obscured by the internal variability that remains in these time series.

Our analysis demonstrates that a reliable assessment of the linearity of the SAM response to forcing in a model requires a large ensemble, which is generally not available in CMIP5, especially for single forcing experiments.

Various studies have also conducted single-model tests on the linearity assumption. *Koch et al.* [2009] found that combined AA and GHG forcings produce a nonlinear response in surface air temperature in the Goddard Institute of Space Studies (GISS) ModelE [*Schmidt et al.*, 2006], but other studies, including *Fyfe et al.* [2012], find that an inferred all-forcing response derived from the linear combination of single forcings (including GHG, AA, and sO_3) does compare favorably to the AF response from CanESM2 (based on five-member ensembles). *Shiogama et al.* [2013], using MIROC3, suggest that linearity holds for temperature responses, but not for precipitation, and *Dong and Zhou* [2014] found that an assumption of linearity works for SST trends in CSIRO-Mk3.6.0 for the period 1870–2005. Ultimately, it seems apparent that analysis of single models in respect to the linearity assumption in the context of the SAM is unlikely to give a complete understanding of the extent of climate forcing nonlinearity, i.e., the extent of nonlinearity is model dependent. We also acknowledge that our linearity conclusions with regards to the SAM metric may not hold for other metrics of SH climate change and, as discussed above, may be sensitive to the methodology used, even for similar metrics in the same model.

Beyond this conclusion, further interpretation becomes difficult. A lack of linearity in the response precludes a quantitative conclusion being made with respect to the contribution of AAs to trends in the SAM index.

There are multiple feedbacks and uncertainties associated with model forcing that are currently not fully understood. This limits the conclusions we can draw but provides direction for future work.

5. Summary and Conclusions

EEMD analysis is performed on a subset of CMIP5 models to identify significant nonlinear trends in the SAM index. Each CMIP5 model is compared to a null model with similar autoregression characteristics to determine the significance of the trend. A Monte Carlo simulation of 1000 null models provides an estimate of significance limits against which IMFs of the CMIP5 models are assessed.

In support of previous studies, we find that the historical SAM trend is strongly positive (5% level or greater) in 15 of 19 CMIP5 models, and the effect of GHG on this trend is significant (at the 5% level or greater) in all 17 models.

We find that while most models show a decrease in the SAM index in response to an increase in global AA, the majority of models do not show a statistically significant influence of AA on the SAM. Only 2 out of 10 models have robust historical decreases in the SAM index due to AA forcing. Other models also show a decrease but not one that is significant across the majority of ensemble members. The lack of consistency across models suggests that we still have a poor understanding of the AA effect on the SAM, but, as the signal-to-noise ratio is poor, this cannot be better understood without a larger number of models providing AA ensemble members. Our 10-model AA ensemble shows that AAs may affect the SAM and that it has the potential to determine the sign of the near-term SAM trend, if the projected rapid near-term decreases in aerosol emissions are realized. However, more work is required to understand the mechanisms behind the response in order for predictions to be reliable. This influence is likely to be small and is difficult to distinguish from internal variability. Large ensembles are required to better identify the SAM response to AA. The poor signal in the existing experiments means that the mechanisms behind the response are unclear. The mechanism linking changes in AA to changes in the SAM needs to be better understood if predictions of the influence of future AA changes on the SAM are to be reliable. Uncertainty in the concentrations and spatial distribution of AAs, combined with diversity in the representation of aerosol-cloud interactions further complicate the interpretation of the SAM response to AA, highlighting the need for more idealized aerosol experiments and better representations of radiative effects.

Our investigations into the linearity of the SAM response to multiple forcings suggest that linearity may be a poor assumption in some models. This makes the quantification of the relative contributions of different forcings to the trends difficult to quantify. However, we also found our analysis to be hampered by internal variability, suggesting that at least 10 ensemble members are required to see a forced response to the SAM.

Acknowledgments

We acknowledge the World Climate Research Programme's Working Group on Coupled Modelling, which is responsible for CMIP, and we thank the climate modeling groups (listed in Table 1 of this paper) for producing and making available their model output (https://pcmdi.llnl.gov/search/cmip5/). For CMIP the U.S. Department of Energy's Program for Climate Model Diagnosis and Intercomparison provides coordinating support and led development of software infrastructure in partnership with the Global Organization for Earth System Science Portals. We also thank the British Atmospheric Data Centre (BADC) for providing access to their CMIP5 data archive and JASMIN and CEDA. We thank Liang Guo for providing the AA simulations for HadGEM2-ES and Nick Dunstone for providing NoAA simulation for HadGEM2-ES (both data sets are available from the authors upon request; email: hamish.steptoe@metoffice.gov.uk). The National Computing Infrastructure, Australia, provided access to additional CSIRO ensemble members (http://dapds00.nci.org.au). We thank Andrew Charlton-Perez and Theo Economou for useful discussions during the preparation of the first draft and two anonymous reviewers for their helpful feedback that greatly improved the final manuscript. H.S. would like to thank the Met Office and Paul Maisey for putting the 20% policy into practice.

References

Albrecht, B. A. (1989), Aerosols, cloud microphysics, and fractional cloudiness, *Science*, *245*(4923), 1227–1230.

Boucher, O., et al. (2013), *Climate Change 2013: The Physical Science Basis. Contribution of Working Group I to the Fifth Assessment Report of the Intergovernmental Panel on Climate Change, Chap. Clouds and Aerosols*, Cambridge Univ. Press, Cambridge, U. K., and New York, doi:10.1017/CBO9781107415324.016.

Box, G. E. P., G. M. Jenkins, and G. C. Reinsel (2008), Time series analysis: Forecasting and control, 4th ed., John Wiley, Hoboken, N. J., doi:10.1002/9781118619193.

Cai, W., D. Bi, J. Church, T. Cowan, M. Dix, and L. Rotstayn (2006), Pan-oceanic response to increasing anthropogenic aerosols: Impacts on the Southern Hemisphere oceanic circulation, *Geophys. Res. Lett.*, *33*, L21707, doi:10.1029/2006GL027513.

Cai, W., and T. Cowan (2007), Trends in Southern Hemisphere circulation in IPCC AR4 models over 1950–99: Ozone depletion versus greenhouse forcing, *J. Clim.*, *20*(4), 681–693, doi:10.1175/JCLI4028.1.

Cai, W., T. Cowan, and M. Thatcher (2012), Rainfall reductions over Southern Hemisphere semi-arid regions: The role of subtropical dry zone expansion, *Sci. Rep.*, *2*, 702, doi:10.1038/srep00702.

Carslaw, K. S., et al. (2013), Large contribution of natural aerosols to uncertainty in indirect forcing, *Nature*, *503*(7474), 67–71, doi:10.1038/nature12674.

Ceppi, P., and D. L. Hartmann (2013), On the speed of the Eddy-Driven jet and the width of the Hadley cell in the Southern Hemisphere, *J. Clim.*, *26*(10), 3450–3465, doi:10.1175/JCLI-D-12-00414.1.

Ceppi, P., Y.-T. Hwang, X. Liu, D. M. W. Frierson, and D. L. Hartmann (2013), The relationship between the ITCZ and the Southern Hemispheric eddy driven jet, *J. Geophys. Res. Atmos.*, *118*, 5136–5146, doi:10.1002/jgrd.50461.

Ceppi, P., M. D. Zelinka, and D. L. Hartmann (2014), The response of the Southern Hemispheric eddy-driven jet to future changes in shortwave radiation in CMIP5, *Geophys. Res. Lett.*, *41*, 3244–3250, doi:10.1002/2014GL060043.

Chang, C. Y., J. C. H. Chiang, M. F. Wehner, A. R. Friedman, and R. Ruedy (2011), Sulfate Aerosol control of tropical Atlantic climate over the twentieth century, *J. Clim.*, *24*(10), 2540–2555, doi:10.1175/2010JCLI4065.1.

Chiang, J. C. H., and A. R. Friedman (2012), Extratropical cooling, interhemispheric thermal gradients, and tropical climate change, *Annu. Rev. Earth Planet. Sci.*, *40*(1), 383–412, doi:10.1146/annurev-earth-042711-105545.

Choi, J., S.-W. Son, J. Lu, and S.-K. Min (2014), Further observational evidence of Hadley cell widening in the Southern Hemisphere, *Geophys. Res. Lett.*, *41*, 2590–2597, doi:10.1002/2014GL059426.
Chylek, P., J. Li, M. K. Dubey, M. Wang, and G. Lesins (2011), Observed and model simulated 20th century Arctic temperature variability: Canadian Earth System Model CanESM2, *Atmos. Chem. Phys. Discuss.*, *11*(8), 22,893–22,907, doi:10.5194/acpd-11-22893-2011.
Cionni, I., V. Eyring, J.-F. Lamarque, W. J. Randel, D. S. Stevenson, F. Wu, G. E. Bodeker, T. G. Shepherd, D. T. Shindell, and D. W. Waugh (2011), Ozone database in support of CMIP5 simulations: Results and corresponding radiative forcing, *Atmos. Chem. Phys.*, *11*(21), 11,267–11,292, doi:10.5194/acp-11-11267-2011.
Davison, A. C., and D. V. Hinkley (1997), Bootstrap methods and their application, Cambridge Univ. Press, Cambridge, U. K., doi:10.1017/CBO9780511802843.
Dong, L., and T. Zhou (2014), The Indian Ocean sea surface temperature warming simulated by CMIP5 models during the twentieth century: Competing forcing roles of GHGs and anthropogenic aerosols, *J. Clim.*, *27*(9), 3348–3362, doi:10.1175/JCLI-D-13-00396.1.
Donner, L. J., et al. (2011), The dynamical core, physical parameterizations, and basic simulation characteristics of the atmospheric component AM3 of the GFDL global coupled model CM3, *J. Clim.*, *24*(13), 3484–3519, doi:10.1175/2011JCLI3955.1.
Dufresne, J. L., et al. (2013), Climate change projections using the IPSL-CM5 Earth System Model: From CMIP3 to CMIP5, *Clim. Dyn.*, *40*(9–10), 2123–2165, doi:10.1007/s00382-012-1636-1.
Dunne, J. P., et al. (2012), GFDL's ESM2 global coupled climate-carbon Earth system models. Part I: Physical formulation and baseline simulation characteristics, *J. Clim.*, *25*(19), 6646–6665, doi:10.1175/JCLI-D-11-00560.1.
Fogt, R. L., J. Perlwitz, A. J. Monaghan, D. H. Bromwich, J. M. Jones, and G. J. Marshall (2009), Historical SAM Variability. Part II: Twentieth-century variability and trends from reconstructions, observations, and the IPCC AR4 Models, *J. Clim.*, *22*(20), 5346–5365, doi:10.1175/2009JCLI2786.1.
Franzke, C. (2009), Multi-scale analysis of teleconnection indices: Climate noise and nonlinear trend analysis, *Nonlinear Processes Geophys.*, *16*(1), 65–76, doi:10.5194/npg-16-65-2009.
Franzke, C. (2012), Nonlinear trends, long-range dependence, and climate noise properties of surface temperature, *J. Climate*, *25*(12), 4172–4183, doi:10.1175/JCLI-D-11-00293.1.
Franzke, C. L. E., T. Graves, N. W. Watkins, R. B. Gramacy, and C. Hughes (2012), Robustness of estimators of long-range dependence and self-similarity under non-Gaussianity, *Philos. Trans. R. Soc. A*, *370*(1962), 1250–1267, doi:10.1098/rsta.2011.0349.
Franzke, C. (2013), Significant reduction of cold temperature extremes at Faraday/Vernadsky station in the Antarctic Peninsula, *Int. J. Climatol.*, *33*(5), 1070–1078, doi:10.1002/joc.3490.
Frölicher, T. L., J. L. Sarmiento, D. J. Paynter, J. P. Dunne, J. P. Krasting, and M. Winton (2015), Dominance of the southern ocean in anthropogenic carbon and heat uptake in CMIP5 models, *J. Clim.*, *28*(2), 862–886, doi:10.1175/JCLI-D-14-00117.1.
Fyfe, J. C., J. C. Fyfe, N. P. Gillett, N. P. Gillett, G. J. Marshall, and G. J. Marshall (2012), Human influence on extratropical Southern Hemisphere summer precipitation, *Geophys. Res. Lett.*, *39*, L23711, doi:10.1029/2012GL054199.
Gent, P. R., et al. (2011), The community climate system model version 4, *J. Clim.*, *24*(19), 4973–4991, doi:10.1175/2011JCLI4083.1.
Gerber, E. P., and S.-W. Son (2014), Quantifying the summertime response of the austral jet stream and Hadley cell to stratospheric ozone and greenhouse gases, *J. Clim.*, *27*(14), 5538–5559, doi:10.1175/JCLI-D-13-00539.1.
Gillett, N. P., J. C. Fyfe, and D. E. Parker (2013), Attribution of observed sea level pressure trends to greenhouse gas, aerosol, and ozone changes, *Geophys. Res. Lett.*, *40*, 2302–2306, doi:10.1002/grl.50500.
Gong, D., and S. Wang (1999), Definition of Antarctic Oscillation Index, *Geophys. Res. Lett.*, *26*(4), 459–462, doi:10.1029/1999GL900003.
Ho, M., A. S. Kiem, and D. C. Verdon-Kidd (2012), The Southern Annular Mode: A comparison of indices, *Hydrol. Earth Syst. Sci.*, *16*(3), 967–982, doi:10.5194/hess-16-967-2012.
Hurrell, J. W., et al. (2013), The community Earth system model: A framework for collaborative research, *Bull. Am. Meteorol. Soc.*, *94*(9), 1339–1360, doi:10.1175/BAMS-D-12-00121.1.
Iversen, T., et al. (2013), The Norwegian Earth System Model, NorESM1-M—Part 2: Climate response and scenario projections, *Geosci. Model Dev.*, *6*(2), 389–415, doi:10.5194/gmd-6-389-2013.
Ji, D., et al. (2014), Description and basic evaluation of BNU-ESM version 1, *Geosci. Model Dev. Discuss.*, *7*(2), 1601–1647, doi:10.5194/gmd-7-2039-2014.
Jones, C. D., et al. (2011), The HadGEM2-ES implementation of CMIP5 centennial simulations, *Geosci. Model Dev.*, *4*(3), 543–570, doi:10.5194/gmd-4-543-2011.
Kidston, J., and E. P. Gerber (2010), Intermodel variability of the poleward shift of the austral jet stream in the CMIP3 integrations linked to biases in 20th century climatology, *Geophys. Res. Lett.*, *37*, L09708, doi:10.1029/2010GL042873.
Kloster, S., F. Dentener, J. Feichter, F. Raes, J. v. Aardenne, E. Roeckner, U. Lohmann, P. Stier, and R. Swart (2008), Influence of future air pollution mitigation strategies on total aerosol radiative forcing, *Atmos. Chem. Phys.*, *8*(21), 6405–6437, doi:10.5194/acp-8-6405-2008.
Koch, D., S. Menon, A. Del Genio, R. Ruedy, I. Alienov, and G. A. Schmidt (2009), Distinguishing aerosol impacts on climate over the past century, *J. Clim.*, *22*(10), 2659–2677, doi:10.1175/2008JCLI2573.1.
Lamarque, J.-F., et al. (2010), Historical (1850–2000) gridded anthropogenic and biomass burning emissions of reactive gases and aerosols: Methodology and application, *Atmos. Chem. Phys.*, *10*(15), 7017–7039, doi:10.5194/acp-10-7017-2010.
Lee, S., and S. B. Feldstein (2013), Detecting ozone- and greenhouse gas-driven wind trends with observational data, *Science*, *339*(6119), 563–567, doi:10.1126/science.1225154.
Limpasuvan, V., and D. L. Hartmann (1999), Eddies and the annular modes of climate variability, *Geophys. Res. Lett.*, *26*(20), 3133–3136, doi:10.1029/1999GL010478.
Mao, K. B., Y. Ma, L. Xia, W. Y. Chen, X. Y. Shen, T. J. He, and T. R. Xu (2014), Global aerosol change in the last decade: An analysis based on MODIS data, *Atmos. Environ.*, *94*, 680–686, Global aerosol change in the last decade: An analysis based on MODIS data.
Marshall, G. J. (2003), Trends in the Southern Annular Mode from observations and reanalyses, *J. Clim.*, *16*, 4134–4143, doi:10.1175/1520-0442(2003)016<4134:TITSAM>2.0.CO;2.
Meinshausen, M., et al. (2011), The RCP greenhouse gas concentrations and their extensions from 1765 to 2300, *Clim. Change*, *109*(1–2), 213–241, doi:10.1007/s10584-011-0156-z.
Pawson, S., W. Steinbrecht, A. J. Charlton-Perez, M. Fujiwara, A. Y. Karpechko, I. Petropavlovskikh, J. Urban, and M. Weber (2014), Update on global ozone: Past, present, and future, in *Scientific Assessment of Ozone Depletion: 2014. Global Ozone Research and Monitoring Project (55)*, edited by A.-L. Ajavon et al., pp. 2.1–2.66, World Meteorol. Organiz., Geneva, Switzerland.
Pohl, B., N. Fauchereau, C. J. C. Reason, and M. Rouault (2010), Relationships between the Antarctic Oscillation, the Madden–Julian Oscillation, and ENSO, and consequences for rainfall analysis, *J. Clim.*, *23*(2), 238–254, doi:10.1175/2009JCLI2443.1.
Polvani, L. M., D. W. Waugh, G. J. P. Correa, and S.-W. Son (2011a), Stratospheric ozone depletion: The main driver of twentieth-century atmospheric circulation changes in the Southern Hemisphere, *J. Clim.*, *24*(3), 795–812, doi:10.1175/2010JCLI3772.1.

Polvani, L. M., M. Previdi, and C. Deser (2011b), Large cancellation, due to ozone recovery, of future Southern Hemisphere atmospheric circulation trends, *Geophys. Res. Lett.*, *38*, L04707, doi:10.1029/2011GL046712.
Quan, X.-W., M. P. Hoerling, J. Perlwitz, H. F. Diaz, and T. Xu (2014), How fast are the tropics expanding?, *J. Clim.*, *27*(5), 1999–2013, doi:10.1175/JCLI-D-13-00287.1.
Rotstayn, L. D. (2013), Projected effects of declining anthropogenic aerosols on the Southern Annular Mode, *Environ. Res. Lett.*, *8*(4), 044028, doi:10.1088/1748-9326/8/4/044028.
Rotstayn, L. D., S. J. Jeffrey, M. A. Collier, S. M. Dravitzki, A. C. Hirst, J. I. Syktus, and K. K. Wong (2012), Aerosol- and greenhouse gas-induced changes in summer rainfall and circulation in the Australasian region: A study using single-forcing climate simulations, *Atmos. Chem. Phys.*, *12*(14), 6377–6404, doi:10.5194/acp-12-6377-2012.
Rotstayn, L. D., M. A. Collier, S. J. Jeffrey, J. Kidston, J. I. Syktus, and K. K. Wong (2013), Anthropogenic effects on the subtropical jet in the Southern Hemisphere: Aerosols versus long-lived greenhouse gases, *Environ. Res. Lett.*, *8*(1), 014030, doi:10.1088/1748-9326/8/1/014030.
Schmidt, G. A., et al. (2006), Present-day atmospheric simulations using GISS ModelE: Comparison to in situ, satellite, and reanalysis data, *J. Clim.*, *19*(2), 153–192, doi:10.1175/JCLI3612.1.
Schmidt, G. A., et al. (2014), Configuration and assessment of the GISS ModelE2 contributions to the CMIP5 archive, *J. Adv. Model. Earth Syst.*, *6*, 141–184, doi:10.1002/2013MS000265.
Shindell, D. T., and G. A. Schmidt (2004), Southern Hemisphere climate response to ozone changes and greenhouse gas increases, *Geophys. Res. Lett.*, *31*, L18209, doi:10.1029/2004GL020724.
Shiogama, H., D. A. Stone, T. Nagashima, T. Nozawa, and S. Emori (2013), On the linear additivity of climate forcing-response relationships at global and continental scales, *Int. J. Climatol.*, *33*(11), 2542–2550, doi:10.1002/joc.3607.
Solman, S. A., and I. Orlanski (2014), Poleward shift and change of frontal activity in the Southern Hemisphere over the last 40 years, *J. Atmos. Sci.*, *71*(2), 539–552, doi:10.1175/JAS-D-13-0105.1.
Sugiura, N. (1978), Further analysts of the data by Akaike' s information criterion and the finite corrections, *Commun. Stat. Theor. Methods*, *7*(1), 13–26, doi:10.1080/03610927808827599.
Taylor, K. E., V. Balaji, S. Hankin, M. Juckes, B. Lawrence, and S. Pascoe (2012), CMIP5 data reference syntax (DRS) and controlled vocabularies, Tech. Rep., World Clim. Res. Program.
Thompson, D. W. J., and S. Solomon (2002), Interpretation of recent Southern Hemisphere climate change, *Science*, *296*(5569), 895–899, doi:10.1126/science.1069270.
Thompson, D. W. J., S. Solomon, P. J. Kushner, M. H. England, K. M. Grise, and D. J. Karoly (2011), Signatures of the Antarctic ozone hole in Southern Hemisphere surface climate change, *Nat. Geosci.*, *4*(11), 741–749, doi:10.1038/ngeo1296.
Twomey, S. (1977), The influence of pollution on the shortwave albedo of clouds, *J. Atmos. Sci.*, *34*(7), 1149–1152, doi:10.1175/1520-0469(1977)034<1149:TIOPOT>2.0.CO;2.
van Vuuren, D. P., et al. (2011), The representative concentration pathways: An overview, *Clim. Change*, *109*(1–2), 5–31, doi:10.1007/s10584-011-0148-z.
Visbeck, M. (2009), A station-based Southern Annular Mode index from 1884 to 2005, *J. Clim.*, *22*(4), 940–950, doi:10.1175/2008JCLI2260.1.
Voldoire, A., et al. (2012), The CNRM-CM5.1 global climate model: Description and basic evaluation, *Clim. Dyn.*, *40*(9–10), 2091–2121, doi:10.1007/s00382-011-1259-y.
Wang, G., W. Cai, and A. Purich (2014), Trends in Southern Hemisphere wind-driven circulation in CMIP5 models over the 21st century: Ozone recovery versus greenhouse forcing, *J. Geophys. Res. Oceans*, *119*, 2974–2986, doi:10.1002/2013JC009589.
Watanabe, M., et al. (2010), Improved climate simulation by MIROC5: Mean states, variability, and climate sensitivity, *J. Clim.*, *23*(23), 6312–6335, doi:10.1175/2010JCLI3679.1.
Watanabe, S., et al. (2011), MIROC-ESM 2010: Model description and basic results of CMIP5-20c3m experiments, *Geosci. Model Dev.*, *4*(4), 845–872, doi:10.5194/gmd-4-845-2011.
Wilcox, L. J., A. J. Charlton-Perez, and L. J. Gray (2012), Trends in Austral jet position in ensembles of high- and low-top CMIP5 models, *J. Geophys. Res.*, *117*, D13115, doi:10.1029/2012JD017597.
Wilcox, L. J., E. J. Highwood, and N. J. Dunstone (2013), The influence of anthropogenic aerosol on multi-decadal variations of historical global climate, *Environ. Res. Lett.*, *8*(2), 024033, doi:10.1088/1748-9326/8/2/024033.
Wilcox, L. J., E. J. Highwood, B. B. B. Booth, and K. S. Carslaw (2015), Quantifying sources of inter-model diversity in the cloud albedo effect, *Geophys. Res. Lett.*, *42*, 1568–1575, doi:10.1002/2015GL063301.
Wu, T., R. Yu, F. Zhang, Z. Wang, M. Dong, L. Wang, X. Jin, D. Chen, and L. Li (2010), The Beijing Climate Center atmospheric general circulation model: Description and its performance for the present-day climate, *Clim. Dyn.*, *34*(1), 123–147, doi:10.1007/s00382-008-0487-2.
Wu, Z., and N. E. Huang (2004), A study of the characteristics of white noise using the empirical mode decomposition method, *Proc. R. Soc. A*, *460*(2046), 1597–1611, doi:10.1098/rspa.2003.1221.
Wu, Z., and N. E. Huang (2009), Ensemble empirical mode decomposition: A noise-assisted data analysis method, *Adv. Adapt. Data Anal.*, *1*(1), 1–41, doi:10.1142/S1793536909000047.
Wu, Z., N. E. Huang, S. R. Long, and C. K. Peng (2007), On the trend, detrending, and variability of nonlinear and nonstationary time series, *Proc. Natl. Acad. Sci. U.S.A.*, *104*(38), 14,889–14,894, doi:10.1073/pnas.0701020104.
Xie, S.-P., B. Lu, and B. Xiang (2013), Similar spatial patterns of climate responses to aerosol and greenhouse gas changes, *Nat. Geosci.*, *6*(10), 828–832, doi:10.1038/ngeo1931.
Yukimoto, S., et al. (2012), A new global climate model of the meteorological research institute: MRI-CGCM3, *J. Meteorol. Soc. Jpn.*, *90A*, 23–64, doi:10.2151/jmsj.2012-A02.
Zelinka, M. D., T. Andrews, P. M. Forster, and K. E. Taylor (2014), Quantifying components of aerosol-cloud-radiation interactions in climate models, *J. Geophys. Res. Atmos.*, *119*, 7599–7615, doi:10.1002/2014JD021710.